Derivation of various transfer functions of ideal or aberrated imaging systems from the three-dimensional transfer function

Joseph J. M. Braat[1] and Augustus J. E. M. Janssen[2]

[1]*Optics Research Group, Faculty of Applied Sciences, Technical University Delft, Lorentzweg 1, 2628 CJ Delft, The Netherlands**

[2]*Department of Mathematics and Computer Science, Eindhoven University of Technology, P.O. Box 513, 5600 MB Eindhoven, The Netherlands*

The three-dimensional frequency transfer function for optical imaging systems has been introduced by Frieden in the 1960's. The analysis of this function and its partly back-transformed functions (two-dimensional and one-dimensional optical transfer functions) in the case of an ideal or aberrated imaging system has received relatively little attention in the literature. Regarding ideal imaging systems with an incoherently illuminated object volume, we present analytic expressions for the classical two-dimensional x-y transfer function in a defocussed plane, for the axial z-transfer function in the presence of defocussing and for the x-z-transfer function in the presence of a lateral shift δy of the incoherent line illumination pattern in object space.

For an aberrated imaging system we use the common expansion of the aberrated pupil function with the aid of Zernike polynomials. It is shown that the line integral appearing in Frieden's three-dimensional transfer function can be evaluated for aberrated systems using a relationship established first by Cormack between the line integral of a Zernike polynomial over a full chord of the unit disk and a Chebyshev polynomial of the second kind. Some new developments in the theory of Zernike polynomials from the last decade allow us to present explicit expressions for the line integral in the case of a weakly aberrated imaging system. We outline a similar, but more complicated, analytic scheme for the case of severely aberrated systems.

OCIS codes: 110.4850, 050.1970, 110.0110, 170.6900

*Corresponding author: j.j.m.braat@tudelft.nl

1. Introduction

The three-dimensional frequency transfer function [1] is the extension of the two-dimensional transfer function for the image formed in a plane in image space that is generally perpendicular to the optical axis. After the advances that took place in the forties and fifties of the 20th century in the field of diffraction theory of optical images, see e.g. [2] and [3], the (two-dimensional) spatial frequency concept in optical imaging was introduced via the pioneering work of Duffieux [4]; it was followed by the interesting application of the spatial filtering technique [5]. The spatial frequency transfer in optical imaging was analyzed in depth in some seminal publications by Hopkins, see [6]-[8], and in his contribution to Ch. 10 in [9]. Not only the imaging of incoherently or coherently illuminated objects was treated by him but also the more general case of partially coherent object illumination, a frequently used intermediate approach in microscopy for achieving optimum image contrast. Numerical evaluations of two-dimensional transfer functions were carried out for defocussed systems and for systems suffering from primary aberrations like spherical aberration [10],[11], coma [12] and astigmatism [13]. For incoherently illuminated objects in an imaging systems with higher order aberration terms, the numerical calculations, basically an autocorrelation of the pupil function, had to be carried out in a careful way because of the highly oscillating phase function close to the rim of the pupil function. Nowadays, most optical design programs provide the user with a means to obtain the two-dimensional 'transverse' transfer function of an optical system.

With the increasing interest in (microscopic) imaging in three dimensions, the need for a more widely applicable optical transfer function arose. Fortunately, a remarkable publication in this direction was written at an early stage [1]. It remained relatively unnoticed until the strong interest in out-of-plane imaging developed, for instance, in the case of high-resolution living cell research. The publication [1] was limited to a small-aperture scalar imaging and considered only the two extreme cases of fully coherent or fully incoherent imaging. The partially coherent imaging condition for three-dimensional frequency transfer was treated in [14]; applications in three-dimensional microscopic imaging are found in [15]-[16], the influence of spherical aberration or an annular pupil geometry in [17]. An overview of the scalar three-dimensional transfer function and some lower-dimensional transfer function examples are found in [18]. The refinements that are needed to describe the three-dimensional transfer function in the case of vector imaging at high numerical aperture are discussed in [19]-[22].

In this paper we first present some analytic results for the 'transverse' x-y transfer function in the presence of defocussing, applied to an ideal imaging systems. The effect of defocussing is equally analyzed for the one-dimensional axial z-transfer function. In the case of the two-dimensional x-z transfer function we give analytic results for the value of this function when the receiving plane in image space is laterally shifted in the y-direction. For an aberrated imaging system, we analytically evaluate the line integral that is encountered in Frieden's original paper. A relatively simple expression is obtained for this line integral if the system is weakly aberrated. For a severely aberrated imaging system, we give the procedure that allows to obtain an analytic result.

The contents of this paper are organized as follows. In Section 2 we define the coordinate systems and the imaging geometry and briefly reproduce the basic results given in [1] for incoherently and coherently illuminated objects. In Section 3 we give the analytic results for ideal imaging systems that were discussed above. Section 4 presents the calculation of the line integral related to the three-dimensional transfer function of an aberrated imaging system and the calculation of the classical two-dimensional optical transfer function (OTF). Section 5 gives the conclusions.

2. The three-dimensional scalar transfer function

In this Section we present a rather detailed introduction to the three-dimensional transfer function with an outline of the approximations involved and the domain of validity of the results. We also keep scrupulously track of all proportionality factors involved between the optical quantities in object, pupil and image space. Keeping track of these factors, we can at will transform (partly) forward and backward between the spatial and the frequency domain and get the identity result after a complete transformation cycle. Although we give the three-dimensional transfer function for both coherent and incoherent illumination, it is on the result for an incoherently illuminated object that we will further elaborate in the remaining part of this paper.

In Fig. 1 we have depicted the geometry of a scalar imaging system that images a certain volume V in object space to a volume V' in image space. The three-dimensional (aberrated) point-spread function of an object point Q is represented by the shaded region around the paraxial image point Q' of Q. This point-spread function is obtained from the diffraction integral related to the diffracted wave present in the exit pupil, centered at E'_0, of the

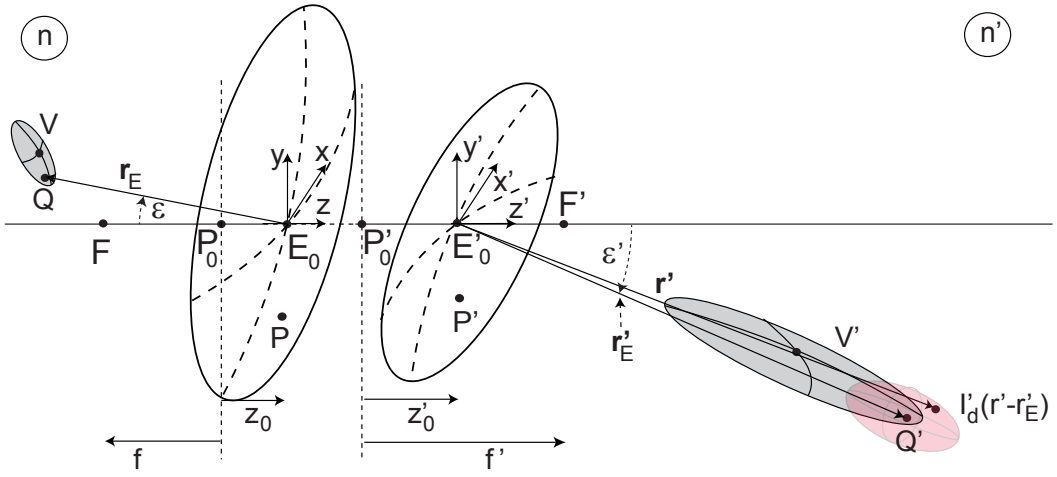

Fig. 1. Imaging of an entire object volume V from object to image space.

imaging system. For a general off-axis object point Q in the volume V at an angle ϵ with the optical axis, we construct the appropriate tilted and rotated coordinate systems that describe the wave incident in the entrance pupil through E_0 and, after propagation through the optical system, its modified version in the exit pupil through E'_0. For a certain volume element V in object space, the imaging aberration introduced by the optical system can be supposed to be stationary with respect to the coordinates (x, y, z) in object space. This means that the point-spread function in image space will be stationary too over the volume element V' that is determined by the paraxial coordinate relationships between these volume elements. It was shown in [1] that in this case the intensity distribution in image space is obtained by a convolution operation of the object intensity distribution and the image-side intensity point-spread function. This holds for an incoherently illuminated object; for a coherently illuminated object, the same reasoning holds with respect to the object amplitude distribution in V and the amplitude point-spread function in image space. In practice, the stationarity of aberration is limited in transverse and axial extent by the ray mapping between object and image space. For the very frequently used Abbe sine condition for the mapping of rays form an axial object point, the stationarity of aberration is large in the transverse direction within an image volume but it can be very limited in the axial direction, even as small as the Rayleigh focal depth.

In the low-aperture scalar imaging approximation, the stationarity of aberration is of no concern as the field angle ϵ is supposed to be negligibly small. This also implies that the

tilt of the pupil reference spheres can be neglected when treating the diffraction problem. It also means that their spherical shape can be sufficiently represented by a parabolic shape. The diffraction integral is then reduced to an integral in which the pathlength differences are approximated by at the most quadratic expressions in the pupil and image coordinates. For the calculation of the diffraction integral of the Fresnel type from exit pupil to image volume we now use the simplified geometry of Fig. 2. The object and image space coordinates of

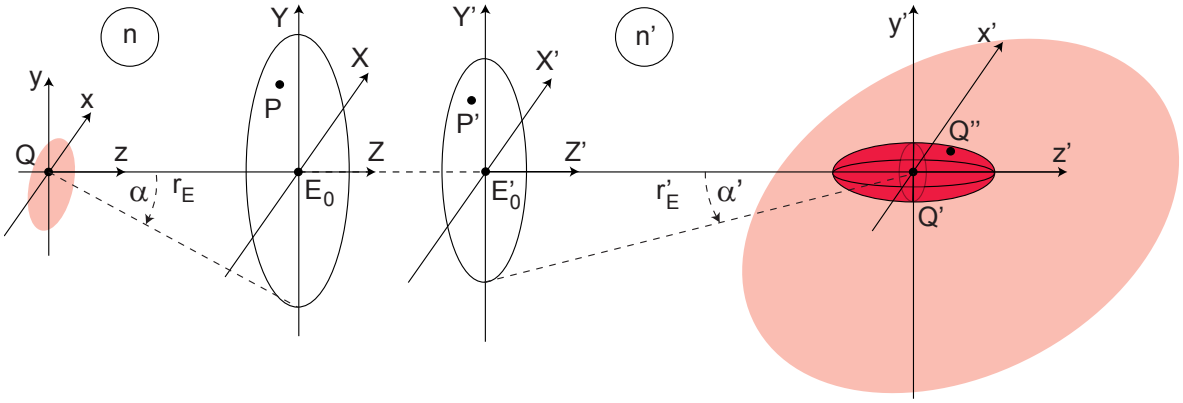

Fig. 2. Definition of coordinates in object and image space for the scalar low-aperture imaging approximation. The shaded object volume is imaged towards the shaded volume in image space. The three-dimensional point-spread function, centered in the origin at Q', originates from the object point Q, and $Q''(x', y', z')$ is a general point of the three-dimensional point-spread function.

an object point Q and its corresponding image point Q' are given in the general picture of Fig. 1 by $(x, y, z)_Q$ for the object point and by $(x', y', z')_{Q'}$ for the paraxial image point Q'. In the simplified geometry of Fig. 2, the oblique auxiliary axis at an angle ϵ' for the imaging of an off-axis object volume has been replaced by the optical axis and Q and Q' coincide with the coordinate origins in object and image space. The coordinates of a general point on the entrance and exit pupil spheres, approximated by the paraboloids with identical curvatures, are given by $(X, Y, Z)_P$ and $(X', Y', Z')_{P'}$; the mapping between P and P' on the pupil surfaces obeys the paraxial imaging laws. The aberrations associated with off-axis imaging are mapped on the exit pupil through E'_0. The spatial frequencies in image space in Fig. 1 are linked to the tilted and rotated coordinate system along the oblique axis at an angle ϵ'. In the low-aperture and small field approximation, these frequencies are identified with the spatial frequencies $(\omega'_x, \omega'_y, \omega'_z)$ defined along the optical axis z' and the lateral axes

x' and y'.

With all these simplifications, the diffraction integral that produces the complex amplitude U'_d of the point-spread function in image space is given by

$$\begin{aligned} U'_d(x',y',z') &= \frac{-i}{\lambda\, r'_E} \iint_{-\infty}^{+\infty} U(X',Y') \exp\left[ik(P'Q'' - P'Q')\right]\, dX'dY' \\ &= \frac{-ik}{2\pi\, r'_E}\, \exp\left\{ik\left(z' + \frac{x'^{\,2} + y'^{\,2}}{2r'_E}\right)\right\}\ \times \\ &\iint_{-\infty}^{+\infty} U(X',Y') \exp\left\{-ik\left[\left(\frac{X'^{\,2} + Y'^{\,2}}{2r'^{\,2}_E}\right) z' \ +\ \frac{X'x' + Y'y'}{r'_E}\right]\right\}\, dX'dY', \end{aligned} \tag{1}$$

with the wavenumber k equal to $2\pi/\lambda$ and $U(X',Y')$ the complex amplitude on the exit pupil sphere of the wave that was issued from a point source in Q in the object plane. The intensity point-spread function I'_d in image space is put equal to $|U'_d|^2$.

To obtain the three-dimensional Fourier transform of the amplitude or intensity distribution, a definition of the elementary plane wave is needed. We write the complex amplitude of a (scalar) plane wave as $A(\boldsymbol{r},t)$=$A_0 \exp[i(\boldsymbol{k}\cdot\boldsymbol{r} - \omega_t t)]$, with $\boldsymbol{k}$ the wave vector and ω_t the time frequency. For the spatial Fourier transform of a general wave with wave function $f(\boldsymbol{r},t)$ and its inverse transform we then have the expression

$$\begin{aligned} F(\boldsymbol{\omega},t) &= \iiint_{-\infty}^{+\infty} f(\boldsymbol{r},t)\ \exp[-i(\boldsymbol{\omega}\cdot\boldsymbol{r})]\, d\boldsymbol{r}\ , \\ f(\boldsymbol{r},t) &= \frac{1}{(2\pi)^3} \iiint_{-\infty}^{+\infty} F(\boldsymbol{\omega},t)\ \exp[+i(\boldsymbol{\omega}\cdot\boldsymbol{r})]\, d\boldsymbol{\omega}\ , \end{aligned} \tag{2}$$

where the sign of the exponential in the inverse transform is in accordance with our definition of the sign of the phase term of an elementary plane wave.

With this definition of the plane wave we work out the three-dimensional Fourier transforms along the lines of [1] to obtain for the incoherent transfer function

$$\begin{aligned} \tilde{I}'_{inc}(\nu'_{x,n},\nu'_{y,n},\nu'_{z,n}) &= \frac{\lambda\, r'^{\,2}_E}{\nu'_{t,n}} \int_A^B U_0\left(\rho_0\left[\frac{\nu'_{t,n}}{2} - \frac{\nu'_{z,n}}{\nu'_{t,n}}\right], \rho_0 Y'_{r,n}\right)\ \times \\ &\qquad U_0^*\left(\rho_0\left[-\frac{\nu'_{t,n}}{2} - \frac{\nu'_{z,n}}{\nu'_{t,n}}\right], \rho_0 Y'_{r,n}\right)\, dY'_{r,n}\ , \end{aligned} \tag{3}$$

with U_0 the lens pupil function in the rotated coordinate system and $2\rho_0$ the pupil diamater. A frequency ν' is given by $\omega'/2\pi$ and the normalized spatial coordinates (x'_n, y'_n, z'_n) and frequencies $(\nu'_{x,n}, \nu'_{y,n}, \nu'_{z,n})$ follow from

$$x'_n = (\sin\alpha'/\lambda)\, x' \ , \qquad y'_n = (\sin\alpha'/\lambda)\, y' \ , \qquad z'_n = (\sin^2\alpha'/\lambda)\, z' \ ,$$
$$\nu'_{x,n} = (\lambda/\sin\alpha')\, \nu'_x \ , \qquad \nu'_{y,n} = (\lambda/\sin\alpha')\, \nu'_y \ , \qquad \nu'_{z,n} = (\lambda/\sin^2\alpha')\, \nu'_z \ , \tag{4}$$

with α' the opening angle of an imaging beam, the radial position r'_n equal to $(x_n^{'2} + y_n^{'2})^{1/2}$ and the transverse frequency $\nu'_{t,n}$ given by $(\nu_{x,n}^{'2} + \nu_{y,n}^{'2})^{1/2}$.

With respect to the analysis in [1] we have chosen the line integral in the exit pupil to be along a rotated Y'-axis, denoted by Y'_r in Fig. 3. The value of $X'_{r,n}$-coordinate of the line l_1 in this rotated coordinate system is fixed, as it is seen from the X-arguments of the pupil functions U_0 and U_0^* in Eq.(3). In the absence of axial modulation in the object, the line l_1 passes through the point P_0 with $X'_{r,n;P_0} = \nu'_{t,n}/2$. The rotation angle θ_ν follows from

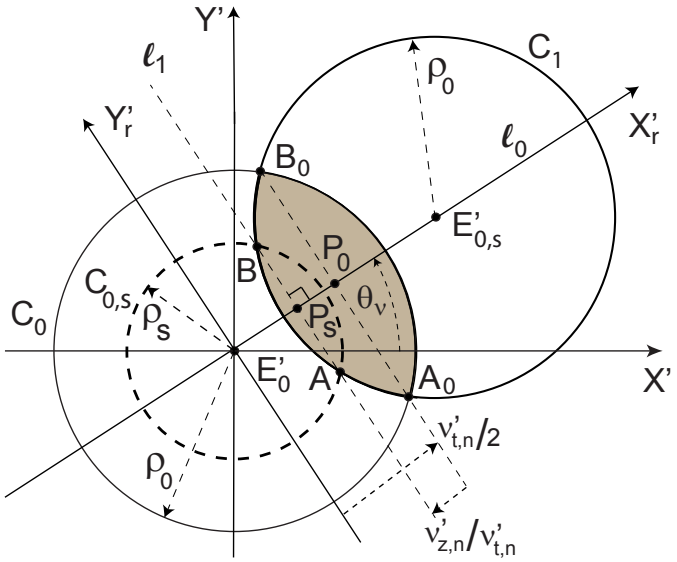

Fig. 3. Example of a line segment AB of line l_1 through P_s, parallel to the Y'_r-axis. A line integral over this segment is needed to obtain the three-dimensional frequency transfer function.

$\cos\theta_\nu = -\nu'_{x,n}/\nu'_{t,n}$ and $\sin\theta_\nu = -\nu'_{y,n}/\nu'_{t,n}$. For a general object showing axial modulation, the location of the line l_1 is determined by the coordinate of the point P_s and the length of $|E'_0 P_s|$ equals

$$X'_{r,n;P_s} = \frac{\nu'_{t,n}}{2} - \frac{\nu'_{z,n}}{\nu'_{t,n}} \ . \tag{5}$$

For an aberration-free imaging system, the length of the line AB in Fig. 3 determines the value of the integral in Eq.(3), yielding,

$$\tilde{I}'_{inc}(\nu'_{t,n}, \nu'_{z,n}) = \frac{2\lambda r_E^{'2}}{\nu'_{t,n}} \sqrt{1 - \left(\frac{\nu'_{t,n}}{2} + \frac{|\nu'_{z,n}|}{\nu'_{t,n}} \right)^2} \ . \tag{6}$$

In this equation we used $|\nu'_{z,n}|$ because the result is symmetric with respect to the line A_0B_0 in the aberration-free case.

In the case of a coherently illuminated object, the three-dimensional transfer function $\tilde{I}'_c$ is given by

$$\tilde{I}'_c(\nu'_{x,n}, \nu'_{y,n}, \nu'_{z,n}) = \frac{-i\lambda^2 r'_E}{\sin^2 \alpha'} \, \delta \left(\nu'_{z,n} - \frac{1}{\sin^2 \alpha'} + \frac{\nu_{x,n}^{'2} + \nu_{y,n}^{'2}}{2} \right) \, U(-\rho_0 \nu'_{x,n}, -\rho_0 \nu'_{y,n}) \ . \tag{7}$$

In Fig. 4 we have plotted the incoherent and coherent three-dimensional transfer functions as a function of the axial and transverse normalized spatial frequencies, $\nu'_{z,n}$ and $\nu'_{t,n}$, respectively. It appears from graph a) and b) that the incoherent and the coherent transfer function have very different ranges of $\nu'_{z,n}$ where they are different from zero. For the transverse frequency $\nu'_{t,n}$ we observe a factor of 2 difference in range between the incoherent and coherent transfer function, a phenomenon that also occurs for the classical two-dimensional transfer function.

3. Lower-dimensional transfer functions derived from the 3D function

In this section we give examples of lower-dimensional transfer functions for an aberration-free system. It is shown that the transfer function of an, on average, defocused three-dimensional image follows in a simple way from the 3D master function.

A. The defocussed two-dimensional transverse transfer function

The first example applies to the two-dimensional transverse frequency transfer function that was at the origin of the frequency analysis of optical systems. In the case of an incoherently illuminated object, the two-dimensional transfer function follows from an inverse transform according to Eq.(2) of $\tilde{I}'_{inc}$ in Eq.(6). The inverse transform is with respect to the axial frequency $\omega'_z = 2\pi\nu'_{z,n} \sin^2 \alpha'/\lambda$. For the aberration-free case we thus obtain the transfer function, with the formal integration interval $[-\infty, +\infty]$,

$$OTF_t(\nu'_{t,n}; z'_n) = 2\rho_0^2 \int \frac{1}{\nu'_{t,n}} \sqrt{1 - \left(\frac{\nu'_{t,n}}{2} + \frac{|\nu'_{z,n}|}{\nu'_{t,n}} \right)^2} \, \exp(+i2\pi\nu'_{z,n} z'_n) \, d\nu'_{z,n} \ . \tag{8}$$

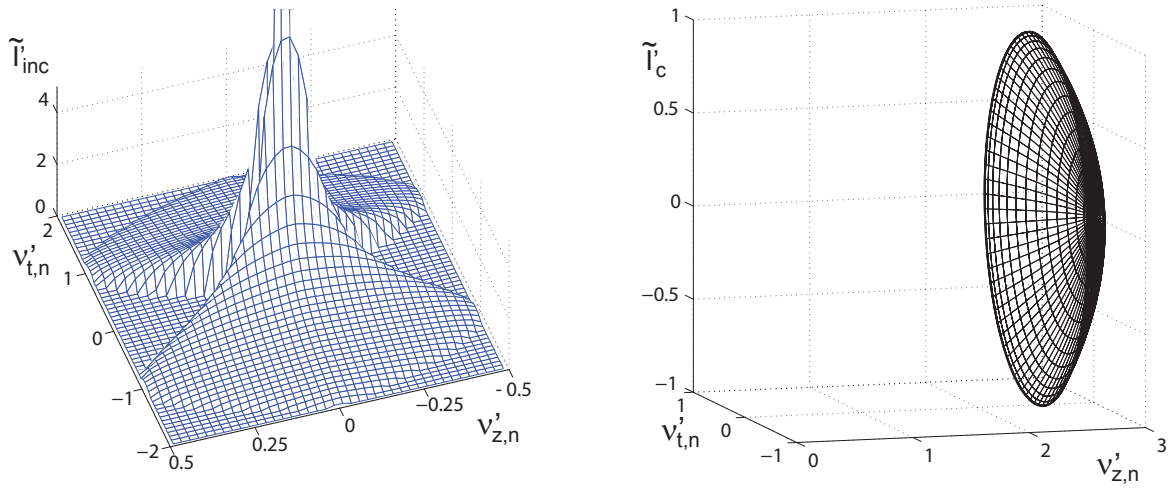

a) b)

Fig. 4. a) The incoherent 3D transfer function $\tilde{I}_{inc}$; the singularity in the graph at the origin has been truncated to a finite value. b) The parabolic surface in space on which the coherent 3D transfer function $\tilde{I}_c$ assumes an infinitely large value ($\alpha' = \pi/6$).

We restrict ourselves to values of $\nu'_{z,n}$ that yield a real-valued square root in the integrand of Eq.(8). The integration limits are then given by $-\nu'_{t,n}(1-\nu'_{t,n}/2) \leq \nu'_{z,n} \leq \nu'_{t,n}(1-\nu'_{t,n}/2)$. This interval is reduced to $0 \leq \nu'_{t,n}(1-\nu'_{t,n}/2)$ if we integrate over twice the real part of the integrand in Eq.(8). With the substitution $\nu'_s = \nu'_{t,n}/2 + |\nu'_{z,n}|/\nu'_{t,n}$ we obtain the expression

$$OTF_t(\nu'_{t,n}; z'_n) = 4\rho_0^2 \, \Re\left\{ \exp(-i\pi \nu'^{\,2}_{t,n} z'_n) \int_{\nu'_{t,n}/2}^{1} \sqrt{1-\nu'^{\,2}_s} \, \exp(+i2\pi \nu'_{t,n} \nu'_s z'_n) \, d\nu'_s \right\}. \qquad (9)$$

The integral is evaluated by making a further substitution $\nu'_s = \cos\phi$. The exponential factor $\exp(+i2\pi\nu'_{t,n} z'_n \cos\phi)$ is expanded using $\exp(ia\cos\phi) = \sum_{m=-\infty}^{+\infty} i^m J_m(a) \exp(im\phi)$. We then obtain the result

$$OTF_t(\nu'_{t,n}; z'_n) = 4\rho_0^2 \, \Re\left\{ \exp(-i\pi \nu'^{\,2}_{t,n} z'_n) \sum_{-\infty}^{+\infty} i^m J_m(2\pi \nu'_{t,n} z'_n) \int_0^{\phi_0} \sin^2\phi \exp(im\phi) \, d\phi \right\}, \qquad (10)$$

with $\phi_0 = \arccos(\nu'_{t,n}/2)$.

The evaluation of the remaining integral yields the result

$$OTF_t(\nu'_{t,n}; z'_n) \;=\; \pi\rho_0^2\,\Re\left\{\frac{2}{\pi}\,\exp(-i\pi\nu'^{\,2}_{t,n} z'_n)\;\sum_{m=-\infty}^{+\infty} i^m\,J_m(2\pi\nu'_{t,n} z'_n)\;\times\right.$$
$$\phi_0\left[\exp\left(\frac{im\phi_0}{2}\right)\mathrm{sinc}\left(\frac{m\phi_0}{2}\right) - \frac{1}{2}\exp\left(\frac{i(m+2)\phi_0}{2}\right)\mathrm{sinc}\left(\frac{(m+2)\phi_0}{2}\right)\right.$$
$$\left.\left. -\frac{1}{2}\exp\left(\frac{i(m-2)\phi_0}{2}\right)\mathrm{sinc}\left(\frac{(m-2)\phi_0}{2}\right)\right]\right\}. \qquad (11)$$

In a different form, this analytic result was already obtained by Hopkins [7] using an integration over the two-circle overlap area of the classical two-dimensional transfer function. Numerical evaluations of the (strongly) defocused two-dimensional OTF_t were presented by Stokseth [23]. For the in-focus incoherent transfer function we get, apart from the leading factor $\pi\rho_0^2$, the classical normalized result for an aberration-free system,

$$OTF_t(\nu'_{t,n}; 0) = \frac{2}{\pi}\,(\phi_0 - \sin\phi_0\cos\phi_0) = \frac{2}{\pi}\,\left[\arccos\left(\frac{\nu'_{t,n}}{2}\right) - \frac{\nu'_{t,n}}{2}\sqrt{1-\left(\frac{\nu'_{t,n}}{2}\right)^2}\right]\;. \qquad (12)$$

The through-focus behavior of the two-dimensional transfer function has been plotted in

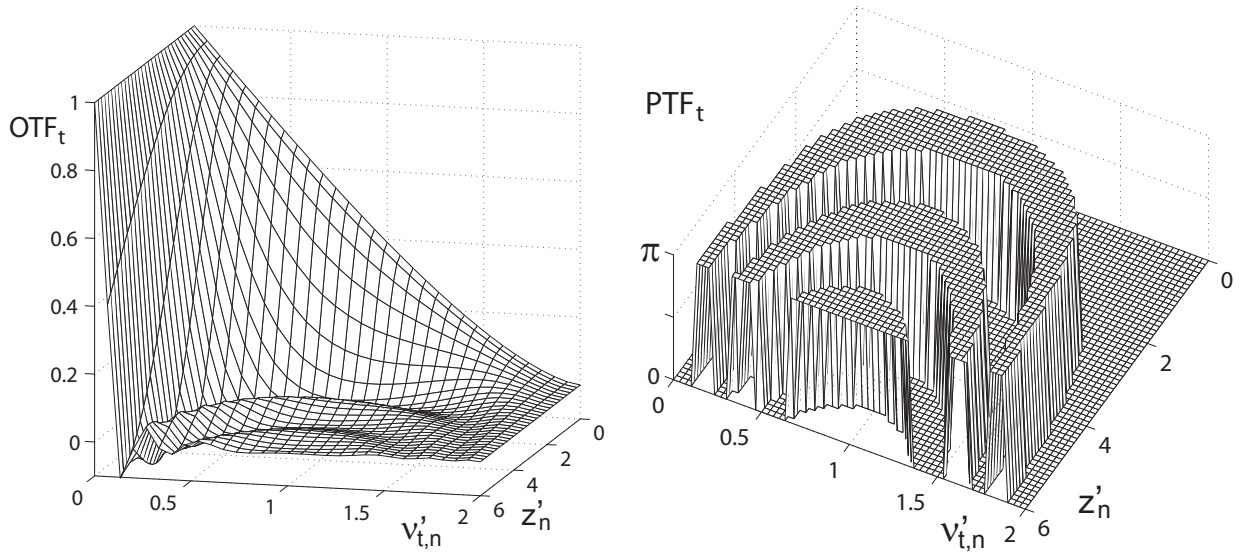

a) b)

Fig. 5. a) The two-dimensional transfer function OTF_t with the defocussing distance z'_n as parameter (aberration-free system). b) The binary phase function PTF_t.

Fig. 5, using Eq.(11). The infinite series has been truncated to a finite number of terms such

that a precision of 10^{-4} has been attained in the real part of the expression in (11). The phase transfer function PTF_t is binary, changing between 0 and π, because OTF_t is a real function and Fig. 5b shows for which values of $\nu'_{t,n}$ the OTF_t changes sign as a function of the defocusing distance z'_n. The foregoing analysis shows that the calculation of the optical transfer function OTF_t by means of a side step via the three-dimensional master function provides us with a simple analytic expression for OTF_t. The standard calculation of OTF_t requires a two-dimensional autocorrelation integral over the common area of two shifted pupil functions.

B. The incoherent axial transfer function in the presence of a lateral off-set

The axial transfer function of an ideal system in the presence of defocussing follows from a double inverse Fourier transform with respect to the frequencies ω'_x and ω'_y of the 3D incoherent transfer function,

$$OTF_z(\nu'_{z,n}; x'_n, y'_n) \;=\; \frac{2\rho_0^2}{\lambda} \iint \frac{1}{\nu'_{t,n}} \sqrt{1 - \left(\frac{\nu'_{t,n}}{2} + \frac{|\nu'_{z,n}|}{\nu'_{t,n}} \right)^2} \;\times \\ \exp\left\{ +i2\pi(\nu'_{x,n} x'_n + \nu'_{y,n} y'_n) \right\} \; d\nu'_{x,n} d\nu'_{y,n} \,, \tag{13}$$

where we used again the normalized spatial coordinates and spatial frequencies. The integration range follows from the requirement that the argument of the square root in the integrand is non-negative. We switch to polar coordinates in the exit pupil and in the image space according to

$$\begin{cases} \nu'_{x,n} = \nu'_{t,n} \cos\theta \,, \\ \nu'_{y,n} = \nu'_{t,n} \sin\theta \,, \end{cases} \qquad \text{and} \qquad \begin{cases} x'_n = r'_n \cos\phi \,, \\ y'_n = r'_n \sin\phi \,. \end{cases} \tag{14}$$

The axial incoherent transfer function is then given by

$$OTF_z(\nu'_{z,n}; r'_n) \;=\; \frac{2\rho_0^2}{\lambda} \int_0^{2\pi} \int \sqrt{1 - \left(\frac{\nu'_{t,n}}{2} + \frac{|\nu'_{z,n}|}{\nu'_{t,n}} \right)^2} \;\times \\ \exp\left\{ +i2\pi\nu'_{t,n} r'_n \cos(\theta - \phi) \right\} \; d\nu'_{t,n} d\theta \;. \tag{15}$$

For the case that $r'_n \equiv 0$, this expression was evaluated in [18]. For the axial frequency transfer of a periodic line object in a position that is laterally shifted over a distance r'_n in the image plane, we need to consider the integrand including the exponential function. The integration with respect to the azimuthal coordinate θ yields $2\pi J_0(2\pi r'_n \nu'_{t,n})$, and the

function OTF_z is then given by,

$$OTF_z(\nu'_{z,n};r'_n) = 2k\rho_0^2 \int \sqrt{1-\left(\frac{\nu'_{t,n}}{2}+\frac{|\nu'_{z,n}|}{\nu'_{t,n}}\right)^2}\, J_0(2\pi r'_n \nu'_{t,n})\, d\nu'_{t,n}\ . \tag{16}$$

For the argument of the square root to be nonnegative, we have the finite integration interval $1-\sqrt{1-2|\nu'_{z,n}|} \le \nu'_{t,n} \le 1+\sqrt{1-2|\nu'_{z,n}|}$ with $0 \le \nu'_{z,n} \le 1/2$. Using the power series expansion of the Bessel function J_0, we get

$$\begin{aligned} OTF_z(\nu'_{z,n};r'_n) &= 2k\rho_0^2 \sum_{m=0}^{\infty} \frac{(-\pi^2 r_n'^2)^m}{(m!)^2} \int_{1-\sqrt{1-2|\nu'_{z,n}|}}^{1+\sqrt{1-2|\nu'_{z,n}|}} \sqrt{1-\left(\frac{\nu'_{t,n}}{2}+\frac{|\nu'_{z,n}|}{\nu'_{t,n}}\right)^2}\, (\nu'_{t,n})^{2m}\, d\nu'_{t,n} \\ &= \pi\rho_0^2\, k\, (1-2|\nu'_{z,n}|)\Bigg\{ 1+2\sum_{m=1}^{M} \frac{(-\pi^2 r_n'^2)^m}{(m!)^2} \sum_{k=0}^{m-1} 2^k \binom{m-1}{k} \ \times \\ &\quad \left(\frac{1}{2}.\frac{3}{3}.\ \cdots\ .\frac{2k+1}{k+2}\right) \left(1-\sqrt{1-2|\nu'_{z,n}|}\right)^{2m-2-2k} \left(1-2|\nu'_{z,n}|\right)^{k/2} \Bigg\}, \end{aligned} \tag{17}$$

where the semi-analytic expression of Appendix A is used for the remaining integral, and the truncation index M is chosen in accordance with the truncation strategy described in the same Appendix.

The normalized axial transfer function OTF_z has been plotted as a function of the spatial frequency $\nu'_{z,n}$ and the lateral off-axis distance r'_n. In the case of a z-modulated line object, the graphs a and b of Fig. 6 show the loss in modulation depth and the phase change when the intensity distribution is decentered with respect to the scanned line over a distance r'_n. The normalization of the transfer function is with respect to the centred situation where the transfer function has a triangular shape. In the case of off-axis scanning, the total intensity incident on a line object becomes less and this is shown by the decrease of the function $OTF_z(r'_n;0)$ for a non-modulated object.

C. The incoherent x-z transfer function for an ideal system

Another transfer function that can be derived from the three-dimensional master transfer function is the $x-z$-transfer function. This transfer function determines the transfer of x- and z-frequency components from a thin modulated object plane with $y = y_0$ to the corresponding (paraxial) image plane with position $y' = y'_0$. The $x-z$ frequency transfer is obtained as a function of the lateral shift of the receiving plane in image space from the nominal position at $y' = y'_0$.

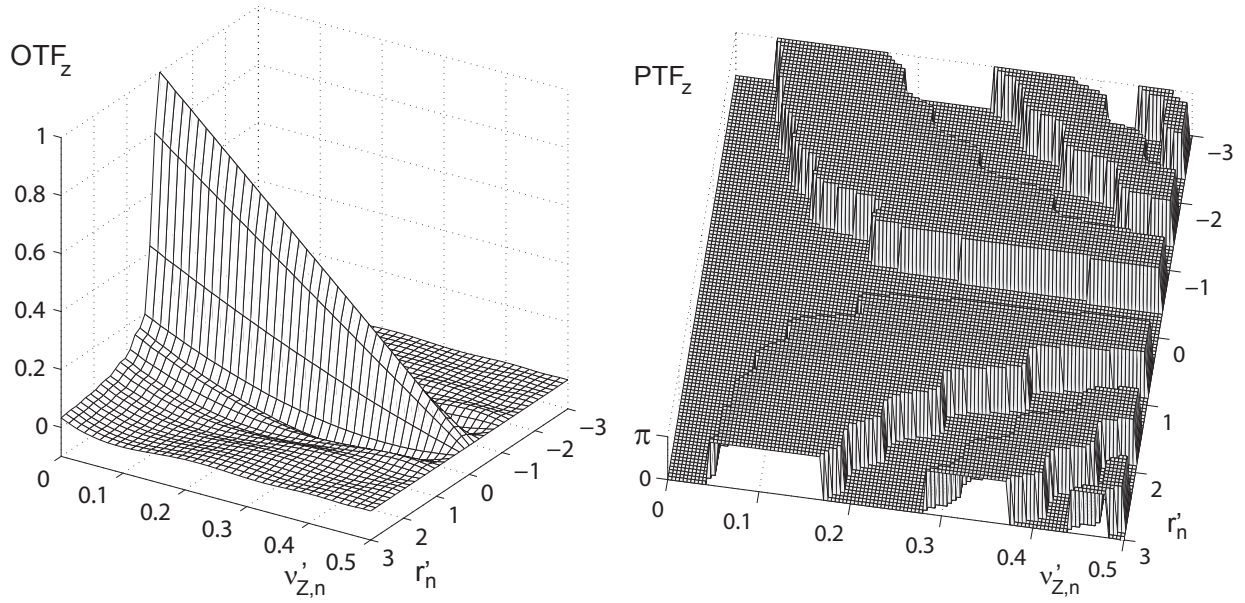

a) b)

Fig. 6. a) The one-dimensional transfer function OTF_z as a function of the transverse off-set r'_n (aberration-free system). b) The corresponding phase function PTF_z.

Carrying out an inverse Fourier transform with respect to the frequency ω'_y of Eq.(6) for the aberration-free case, we obtain

$$OTF_{xz}(\nu'_{x,n}, \nu'_{z,n}; y'_n) = \frac{2\rho_0^2}{\sin\alpha'} \int \frac{1}{\nu'_{t,n}} \sqrt{1 - \left(\frac{\nu'_{t,n}}{2} + \frac{|\nu'_{z,n}|}{\nu'_{t,n}}\right)^2} \exp(+i2\pi\nu'_{y,n} y'_n)\, d\nu'_{y,n} \ , \quad (18)$$

with integration over all $\nu'_{y,n}$ so that the square root is positive real and with $\nu'_{t,n} = (\nu'^2_{x,n} + \nu'^2_{y,n})^{1/2}$. The integral allows an analytic solution for the centered case, with $y' = 0$. The general case, including the exponential factor, can be treated by expanding this exponential into powers of $\nu'_{y,n}$. The first two factors depend on $\nu'_{t,n}$ and are, therefore, even in the integration variable $\nu'_{y,n}$; taking into account the integration range, only even terms in the expansion of the exponential factor need to be retained. With the shorthand writing $s = \nu'_{x,n}$, $v = \nu'_{y,n}$ and $w = |\nu'_{z,n}|$ we have the expression

$$I(s, w; y'_n) = \frac{2\rho_0^2}{\sin\alpha'} \sum_{m=0}^{\infty} \frac{(i2\pi y'_n)^{2m}}{(2m)!} \int \frac{1}{s^2 + v^2} \sqrt{s^2 + v^2 - \left(\frac{s^2 + v^2}{2} + w\right)^2}\, v^{2m}\, dv \, . \quad (19)$$

The remaining integral in Eq.(19), denoted by $I_m(s, w)$, is evaluated in Appendix B.0. The upper index M of the summation over m is established along the same lines as it was done for the summation in Eq.(17).

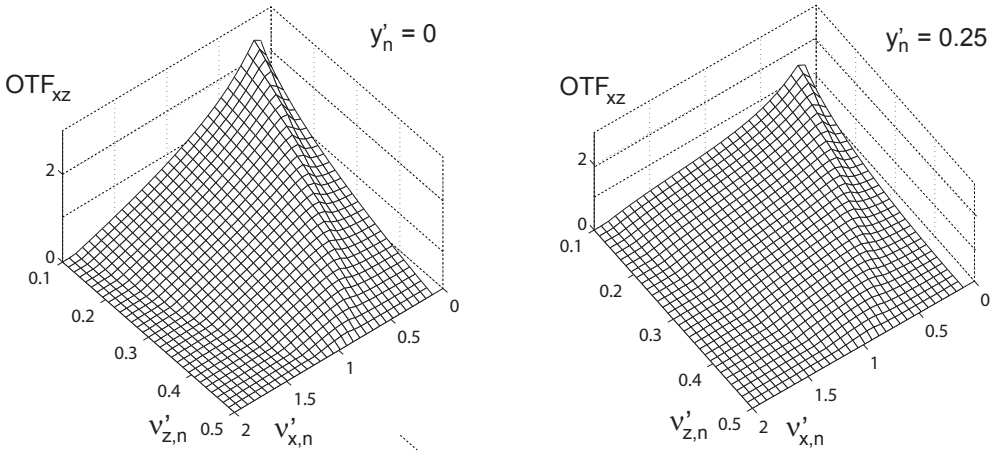

a) b)

Fig. 7. a) Surface plots of the incoherent $x-z$ transfer function $OTF(\nu'_{x,n}, \nu'_{z,n}, y'_n)$ as a function of the off-set y'_n of the three-dimensional point-spread function in the y-direction. Graph a): y'_n=0 ; graph b): y'_n=0.25 .

In Fig. 7 we present two surface plots of the function OTF_{xz} for the parameter values $y'_n = 0$ and 0.25. We have a thin object confined to the plane $y = 0$ that is illuminated by means of an incoherent line parallel to the plane $y = 0$. With the aid of Eq.(19) we calculate the intensity modulation depth measured in image space in the plane $y' = 0$ as a function of the perpendicular distance y of the incoherent line illumination in object space from the plane $y = 0$. In normalized diffraction units, this perpendicular distance amounts to y'_n in image space. From the figure we observe the expected decrease in modulation depth when shifting the illumination by an amount of 0.25 diffraction units off-plane. The representation of $OTF_(\nu'_{x,n}, \nu'_{z,n}; y'_n)$ had to be limited to finite values of $(\nu'_{x,n}, \nu'_{z,n})$. At the origin, the function OTF_{xz} is singular. This means that, close to the origin, the semi-analytic expression for the integral $I_m(s, w)$ that was given in Appendix B.0 shows a slow convergence to its end value and that a large number of terms has to be included in the power series summations.

4. The incoherent 3D transfer function of an aberrated imaging system

In this section we address the computation of the three-dimensional transfer function of an aberrated imaging system, as given by Eq.(3) for the case of incoherent object illumination. Previous work in this field can be found in Sheppard & Hole [25]. They present analytic results for distinct weak aberration terms that affect the phase of the transfer function. We

follow a different path and exploit a specific result for line integrals over the unit disk of Zernike polynomials. Our approach allows the calculation of the transfer function of both weakly and strongly aberrated imaging systems. With reference to Fig. 8a, a one-dimensional integral has to be evaluated along a general line l_1 that intersects the unit disk C at the rim

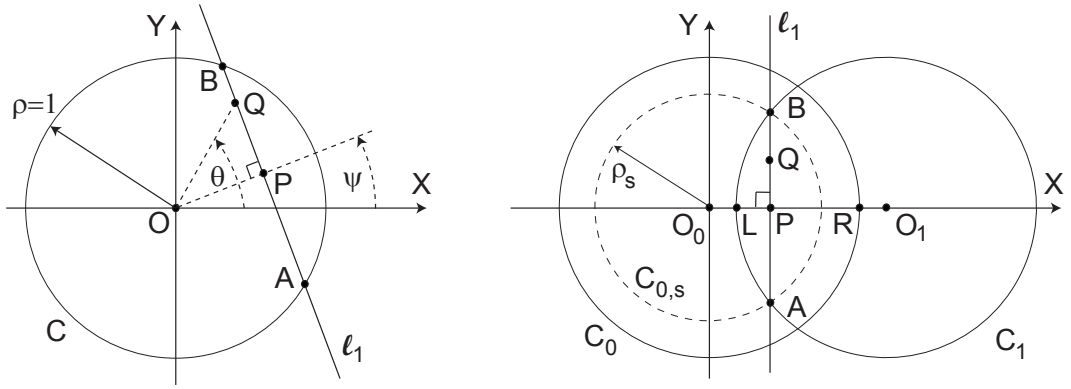

Fig. 8. a) The line integral from A to B along l_1 over a disk with circular rim C. b) The line integral along l_1 related to the common area of two pupil functions C_0 and C_1 with their centers at O_0 and O_1, respectively.

points A and B. The perpendicular distance OP from the origin O to l_1 is denoted by τ and the azimuth of OP with respect to the reference axis X is ψ. A general point Q on the line segment AB is given by its cartesian coordinates $\boldsymbol{r} = (X, Y)$ or its polar coordinates (ρ, θ) with $X + iY = \rho \exp(i\theta)$. The radius of the disk is normalized to unity so that $0 \leq \rho \leq 1$. In the case of an aberrated imaging system, we normalize the transverse dimension of the physical pupil by means of the value ρ_0, such that the radial polar coordinate ρ equals unity on the pupil rim. After normalization of the radial coordinate, the complex amplitude U_0 of the pupil function in Eq.(3) is represented by $U_0'(X, Y)$. This function U_0' is expanded with the aid of Zernike polynomials $Z_k^l(X, Y)$,

$$U_0'(X, Y) = \sum_{k,l} \beta_k^l \, Z_k^l(X, Y) = \sum_{k,l} \beta_k^l \, R_k^{|l|}(\rho) \, \exp(il\theta) \, , \tag{20}$$

with the lower index k running from $k = 0$ up to a maximum degree k_m and $|l| \leq k$, $k - |l|$ even. We should make a remark here on a rotation of the aberration function in Fig. 8b with respect to the X-axis (equal to the $X_{r,n}'$ in Fig. 3). The rotation angle between the $X_{r,n}'$-axis and the reference axis in Fig. 3 is given by θ_ν. This means that the azimuthal

angle θ in a specific Zernike polynomial Z_k^l has to be replaced by $\theta+\theta_\nu$. Taking into account this rotation of the aberration function in Fig. 8b, a general expansion coefficients β_k^l has to be multiplied by a factor $\exp(il\theta_\nu)$.

The expansion above is useful because an interesting analytic result is available for a line integral of $Z_k^l(X,Y)$ between two points on the rim of the unit disk (A and B constitute a full chord of the circular rim of the unit disk C). The analytic result originates from the Radon transform theory in medical imaging [26]-[29] and reads

$$\int\limits_{(X,Y)\,\in\, l_1(\tau,\psi)} Z_k^l(X,Y)\,dp = \frac{2}{k+1}\,(1-\tau^2)^{1/2}\,U_k(\tau)\,\exp(il\psi)\;, \tag{21}$$

with dp the infinitesimal path increment along the line l_1. The polynomial $U_k(x)$, not to be confounded with the amplitude function U_0, is the Chebyshev polynomial of the second kind, $U_k(x)=\sin[(k+1)\alpha]/\sin\alpha$, with $x=\cos\alpha$ [24].

To evaluate the line integral in Eq.(3) we need an expression in terms of Zernike polynomials of the product of two complex amplitude distributions U_0', associated with a centered pupil and a shifted version of it, both with identical expansion coefficients. The position of the two pupils has been depicted in Fig. 8b and pertains to the rotated coordinate system $(X'_{r,n}, Y'_{r,n})$ of Fig. 3; for ease of notation, this coordinate system has been denoted by (X,Y) in Fig. 8. In the rotated coordinate system, the line l_1 is parallel to the Y-axis in Fig. 8b. For compactness of notation, we denote the coordinates of a general point on the unit disk C_0 of Fig. 8b by means of the position vector $\boldsymbol{r}=(X,Y)=\rho\exp(i\theta)$ and the coordinates of the center O_1 of the shifted pupil by the vector $\boldsymbol{a}$.

The line segment AB along which the line integral of Eq.(3) has to be evaluated is a full chord of the circle that delimits the disk C_1 and also a full chord of the disk $C_{0,s}$ with reduced radius ρ_s and centered on O_0. It follows from Fig. 3 that ρ_s is given by

$$\rho_s=\sqrt{1-2|\nu'_{z,n}|}\;, \tag{22}$$

with the special case $\nu'_{t,n}=1$, $|\nu'_{z,n}|=1/2$ for which the scaled disk with rim $C_{0,s}$ is reduced to a point. If negative values of $\nu'_{z,n}$ are considered, the roles of C_0 and C_1 are interchanged in the sense that AB is now a full chord of the disk C_0 and of a disk $C_{1,s}$ that is a scaled version of C_1 with the scaling factor following again from Eq.(22).

The integrand of the line integral in Eq.(3) is written as $U_0'(\boldsymbol{r})\,U_0'^{*}(\boldsymbol{r}-\boldsymbol{a})$. The vector $\boldsymbol{r}$

corresponding to a general point Q on l_1 and the vector $\boldsymbol{a}$ are given by

$$\boldsymbol{r} = (\nu'_{t,n}/2 - \nu'_{z,n}/\nu'_{t,n}, Y) \;, \qquad \boldsymbol{a} = (\nu'_{t,n}, 0) \;. \tag{23}$$

In the following subsections we use the result of Eq.(21) to evaluate the line integral in Eq.(3). We will discriminate between weakly aberrated imaging systems and heavily aberrated ones.

A. Weakly aberrated imaging system

In the case of a weakly aberrated imaging system, the leading term in the expansion of Eq.(20), with coefficient β_0^0 and $Z_0^0(\boldsymbol{r}) = 1$ for $|\boldsymbol{r}| < 1$ and 0 otherwise, dominates all others. For sufficiently small coefficients β_k^l it is allowed to use the following approximate expression

$$\begin{aligned} U'_0(\boldsymbol{r})\, U_0^{'*}(\boldsymbol{r}-\boldsymbol{a}) \;\approx\; |\beta_0^0|^2\, Z_0^0(\boldsymbol{r})\, Z_0^{0*}(\boldsymbol{r}-\boldsymbol{a}) + \sum_{k,l} \beta_0^0\, \beta_k^{l*}\; Z_0^0(\boldsymbol{r})\, Z_k^{l*}(\boldsymbol{r}-\boldsymbol{a}) \\ + \sum_{k,l} \beta_k^l\, \beta_0^{0*} Z_k^l(\boldsymbol{r})\, Z_0^{0*}(\boldsymbol{r}-\boldsymbol{a}) \;, \end{aligned} \tag{24}$$

where in the summations over k, l the term with $k = l = 0$ should be omitted.

After the insertion of the expressions for the vectors $\boldsymbol{r}$ and $\boldsymbol{a}$ in Eq.(24) and using that $Z_0^0(\boldsymbol{r}) = 1$ for $|\boldsymbol{r}| < 1$, the integration of this expression along the line segment AB yields, respectively, the following terms for a particular Zernike term with indices (k, l) in the expansion of U'_0,

$$\begin{aligned} &a) \qquad I_a = f_3\, |\beta_0^0|^2 \int_A^B dY = f_3\, |\beta_0^0|^2\, |AB| = 2 f_3\, |\beta_0^0|^2 \sqrt{1 - \left(\tfrac{\nu'_{t,n}}{2} + \tfrac{\nu'_{z,n}}{\nu'_{t,n}}\right)^2} \;, \\ &b) \qquad I_b = f_3\, \beta_0^0\, \beta_k^{l*} \int_A^B Z_k^{l*}(-\nu'_{t,n}/2 - \nu'_{z,n}/\nu'_{t,n}\,,\, Y)\, dY \;, \\ &c) \qquad I_c = f_3\, \beta_0^{0*}\, \beta_k^l \int_A^B Z_k^l(\nu'_{t,n}/2 - \nu'_{z,n}/\nu'_{t,n}\,,\, Y)\, dY \;, \end{aligned} \tag{25}$$

with $f_3 = \lambda r_E^{'2}/\nu'_{t,n}$ the leading factor in front of the line integral of Eq.(3).

When we apply the result of Eq.(21) to the integral I_b, we obtain

$$I_b = f_3\, \frac{2\beta_0^0\, \beta_k^{l*}}{k+1} \left[1 - \left(\nu'_{t,n}/2 + \nu'_{z,n}/\nu'_{t,n}\right)^2\right]^{1/2} U_k\left(\nu'_{t,n}/2 + \nu'_{z,n}/\nu'_{t,n}\right) \exp(il\pi) \;, \tag{26}$$

where the exponential factor $\exp(-il\pi) = (-1)^l$ stems from the fact that the X-argument of Z_k^{l*} is negative in the case of I_b.

For the line integral I_c in Eq.(25), the segment AB is a full chord of the circle $C_{0,s}$ with reduced radius ρ_s. The value of τ to be employed in Eq.(21) is thus given by $\tau_s = (\nu'_{t,n}/2 -$

$\nu'_{z,n}/\nu'_{t,n})/\rho_s$ and the angle ψ equals zero. For the analytic result of Eq.(21) to be applicable to this line integral, we have to transform the Zernike expansion of the pupil function on the full disk C_0 to an expansion on the disk $C_{0,s}$ with reduced radius ρ_s. For a single Zernike polynomial defined on the unit disk we have the following concise expression for its expansion in Zernike polynomials defined on a disk with reduced size (radius ρ_s), [30],

$$Z_k^l(\rho,\theta) = Z_k^l\left(\rho_s\,\frac{\rho}{\rho_s},\theta\right) = \sum_{k'=|l|,|l|+2,\,\cdots,k}\left[R_k^{k'}(\rho_s) - R_k^{k'+2}(\rho_s)\right]\; Z_{k'}^l\left(\frac{\rho}{\rho_s},\theta\right)\;, \tag{27}$$

with $0 \le \rho \le \rho_s$ and $R_k^{k+2}(\rho) = 0$. The line integral I_c is now written as

$$\begin{aligned} I_c &= f_3\,\beta_0^{0\,*}\beta_k^l \int_A^B Z_k^l(\nu'_{t,n}/2 - \nu'_{z,n}/\nu'_{t,n}\,,\,Y)\,dY \\ &= f_3\,\rho_s\,\beta_0^{0\,*}\beta_k^l \int_A^B Z_k^l\left[\rho_s\left(\nu'_{t,n}/2 - \nu'_{z,n}/\nu'_{t,n}\right)/\rho_s, \rho_s\,(Y/\rho_s)\right]\,(dY/\rho_s) \\ &= f_3\,\rho_s\,\beta_0^{0\,*}\beta_k^l \sum_{k'=|l|,|l|+2,\cdots,k}\left[R_k^{k'}(\rho_s) - R_k^{k'+2}(\rho_s)\right]\int_{A'}^{B'} Z_{k'}^l\left\{\left(\nu'_{t,n}/2 - \nu'_{z,n}/\nu'_{t,n}\right)/\rho_s, Y_s\right\}\,dY_s, \end{aligned} \tag{28}$$

where the coordinates (X_s, Y_s) are the normalized coordinates on the disk $C_{0,s}$ and where the primes attached to the integration endpoints A and B imply that the coordinates of A and B are now expressed in these normalized coordinates $(\rho/\rho_s, \theta)$ on $C_{0,s}$. Using the result of Eq.(21), we finally obtain

$$\begin{aligned} I_c \;=\; 2f_3\,\rho_s\,\beta_0^{0\,*}\beta_k^l \sum_{k'=|l|,|l|+2,\cdots,k} \epsilon_l\,\frac{\left[R_k^{k'}(\rho_s) - R_k^{k'+2}(\rho_s)\right]}{k'+1}\sqrt{1 - \frac{1}{\rho_s^2}\left(\frac{\nu'_{t,n}}{2} - \frac{\nu'_{z,n}}{\nu'_{t,n}}\right)^2} \;\times \\ U_{k'}\left\{\frac{1}{\rho_s}\left(\frac{\nu'_{t,n}}{2} - \frac{\nu'_{z,n}}{\nu'_{t,n}}\right)\right\}\,, \end{aligned} \tag{29}$$

with the quantity ϵ_l defined by the sign of $\nu'_{t,n}/2 - \nu'_{z,n}/\nu'_{t,n}$ according to

$$\epsilon_l \;=\; \begin{cases} 1, & \nu'_{z,n} \le \nu'^{\,2}_{t,n}/2 \\ \exp(il\pi)\,, & \nu'_{z,n} > \nu'^{\,2}_{t,n}/2 \end{cases}\;. \tag{30}$$

The three-dimensional transfer function $\tilde{I}'(\nu'_{t,n}, \nu'_{z,n})$ is obtained by a summation over all the terms of the Zernike expansion of the contributions I_a, I_b and I_c. We obtain the expression

$$\tilde{I}'(\nu'_{t,n}, \nu'_{z,n}) = \frac{2\lambda r_E'^2}{\nu'_{t,n}} |\beta_0^0|^2 \sqrt{1 - \left(\frac{\nu'_{t,n}}{2} + \frac{\nu'_{z,n}}{\nu'_{t,n}}\right)^2} \quad \times$$
$$\left[1 + \sum_{k,l} \left\{ \left(\frac{\beta_k^l}{\beta_0^0}\right)^* \frac{U_k\left(\frac{\nu'_{t,n}}{2} + \frac{\nu'_{z,n}}{\nu'_{t,n}}\right) \exp(il\pi)}{k+1} + \rho_s \left(\frac{\beta_k^l}{\beta_0^0}\right) \quad \times \right.\right.$$
$$\left.\left. \sum_{k'=|l|,|l|+2,\ldots,k} \epsilon_l \frac{\left[R_k^{k'}(\rho_s) - R_k^{k'+2}(\rho_s)\right]}{k'+1} \frac{\sqrt{1 - \frac{1}{\rho_s^2}\left(\frac{\nu'_{t,n}}{2} - \frac{\nu'_{z,n}}{\nu'_{t,n}}\right)^2}}{\sqrt{1 - \left(\frac{\nu'_{t,n}}{2} + \frac{\nu'_{z,n}}{\nu'_{t,n}}\right)^2}} U_{k'}\left[\frac{1}{\rho_s}\left(\frac{\nu'_{t,n}}{2} - \frac{\nu'_{z,n}}{\nu'_{t,n}}\right)\right] \right\}\right] . \tag{31}$$

B. Imaging system with large aberration

We consider now the general case in which the dominance assumption of the $(k,l) = (0,0)$-term in the Zernike expansion of U'_0 is not valid. The treatment of this case is more involved and we will only sketch the general approach without giving all the details of the calculation of coefficients of certain essential function expansions. For the case with larger aberration of the imaging system, it is required to evaluate the line integral of the cross-terms that were neglected in the approximate expression for the integrand of Eq.(24). The line integral of a general term is given by

$$I_d = f_3\, \beta_{k''}^{l''}\, \beta_k^{l\,*} \int_A^B Z_{k''}^{l''}(\boldsymbol{r})\, \left(Z_k^l(\boldsymbol{r} - \boldsymbol{a})\right)^*\, d\boldsymbol{r} \tag{32}$$

and we have to consider all possible combinations of integers (k'', l'') and (k,l) with $k'' - |l''|$ and $k - |l|$ even and non-negative (an exception being made for the case that $k'' = l'' = 0$ or $k = l = 0$). The vector components of $\boldsymbol{r}$ and $\boldsymbol{a}$ were given in Eq.(23) and we have that $d\boldsymbol{r} = (0, dY)$.

Using the extension of [31], Theorem 3.1 (described after its proof), to the case of unrestricted values of $|\boldsymbol{r}|$ and $|\boldsymbol{a}|$ with $Z_k^l(\boldsymbol{r}) = R_k^{|l|}(\rho)\exp(il\theta)$ extended to all $\rho > 0$ accordingly, we can write

$$Z_k^l(\boldsymbol{r} - \boldsymbol{a}) = \sum_{k',l'} D_{k\,k'}^{l\,l'}\, Z_{k'}^{l'}(\boldsymbol{r}) \;, \tag{33}$$

with explicit, finitely many non-zero, but possibly large coefficients D. Inserting this into the integral in Eq.(32), the products $Z_{k''}^{l''}(\boldsymbol{r})\left(Z_{k'}^{l'}(\boldsymbol{r})\right)^*$ show up. These products can be

linearized using the Clebsch-Gordan coefficients related quantities C, see [32],[33],

$$Z_{k''}^{l''}(\boldsymbol{r})\,\left(Z_{k'}^{l'}(\boldsymbol{r})\right)^{*} = Z_{k''}^{l''}(\boldsymbol{r})\,Z_{k'}^{-l'}(\boldsymbol{r}) = \sum_{k'''} C_{k'',k',k'''}^{l'',-l',l''-l'}\;\; Z_{k'''}^{l''-l'}(\boldsymbol{r})\;, \tag{34}$$

and then the result in Eq.(21) can be used to evaluate the integrals $\int_A^B\; Z_{k'''}^{l''-l'}(\boldsymbol{r})\,d\boldsymbol{r}$. This concludes the outline of the computation of the transfer function of a heavily aberrated imaging system.

In Fig. 9 we show an example of a three-dimensional transfer function of a heavily aberrated imaging system. Third-order comatic aberration has been simulated by means of the Zernike coefficients $\beta_3^1 = \beta_3^{-1} = i$, with the coma tail in image space being oriented along the $X'_{r,n}$-axis. These two lowest order expansion coefficients of the complex pupil function do not exactly represent the wave aberration exponential but they are sufficient to show the effect of a large aberration on the transfer function. The numerically calculated values of the transfer function and the analytical results have not been shown separately, the only difference being the numerical accuracy involved. The figure shows that the frequency transfer is hardly affected by the large aberration when the frequency combination $(\nu'_{t,n}, \nu'_{z,n})$ is close to the cut-off region. As it is the case for the classical transfer function OTF_t in the presence of aberration, the largest degradation is observed for the mid-spatial frequencies.

C. The aberrated OTF_{xy} obtained from the three-dimensional transfer function

We use the analytic expression for the line integral occurring in the three-dimensional transfer function of an aberrated system to calculate the classical two-dimensional OTF_{xy}; this was already done for the non-aberrated case in Subsect. 3 A to obtain the values of the transfer function in a defocused plane. Referring to Fig. 8b, we observe that the overlap integral over the common area of the two disks C_0 and C_1 can be obtained by sweeping the line integral AB through the general point P from the point R to L, these points corresponding to the minimum and the maximum allowed values of $\nu'_{z,n}$. For a single Zernike aberration term, we have to calculate the integral over $\nu'_{z,n}$ of I_a, I_b and I_c in the case of weak aberration and also over I_d for heavily aberrated imaging systems. As an example, we consider the integral of I_b from the central point of the segment LR to the extreme point L; this corresponds to the integration interval $[0 \le \nu'_{z,n} \le (1 - \nu'_{t,n}/2)\,\nu'_{t,n}]$. The resulting

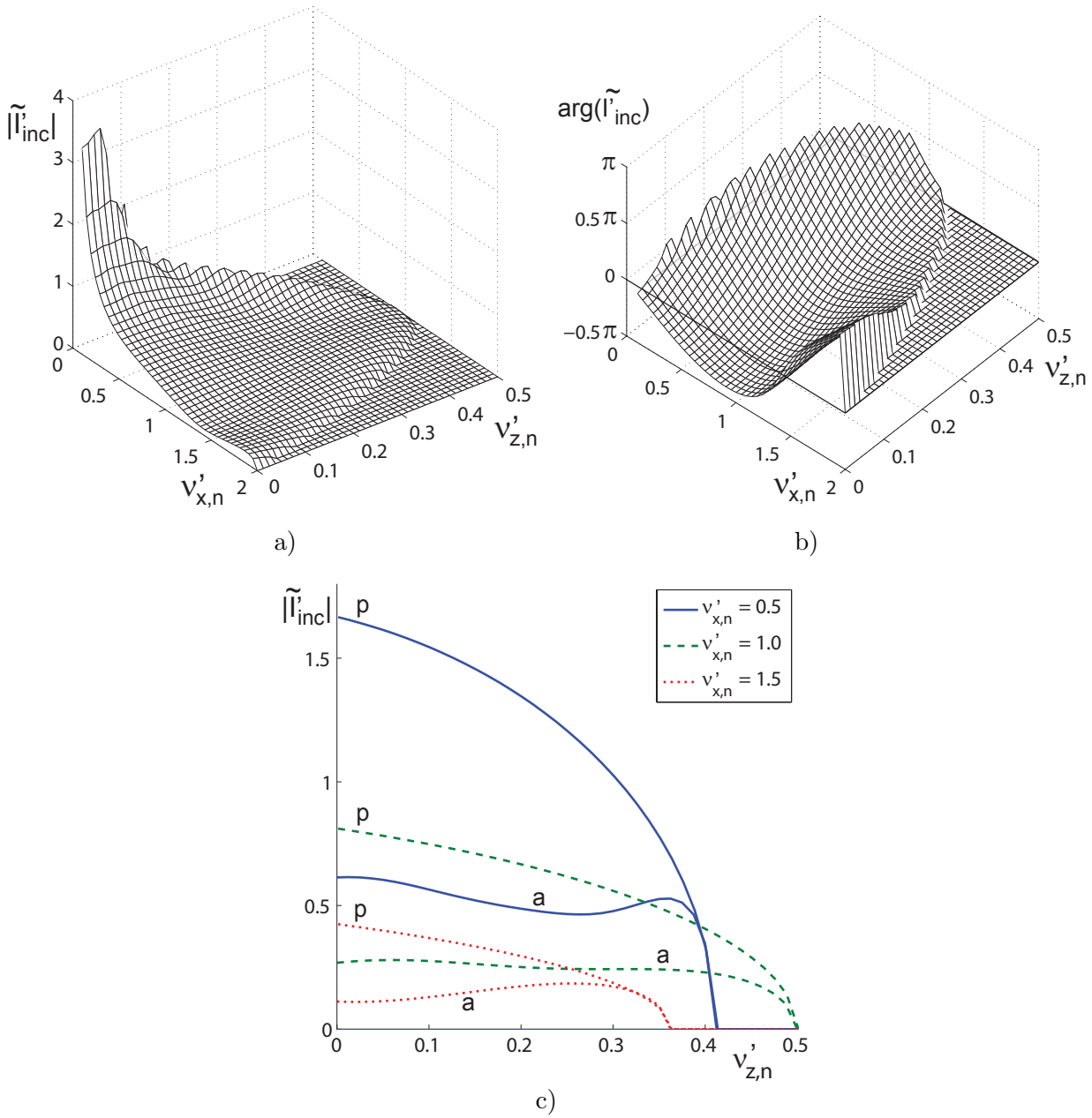

Fig. 9. a) A surface plot of the modulus of the aberrated three-dimensional transfer function $\tilde{I}'_{inc}$ as a function of the (positive) frequencies $(\nu'_{x,n}, 0, \nu'_{z,n})$ with $\nu'_{x,n} \geq 0.1$. b) The argument of the transfer function. c) Three cross-sections of $|\tilde{I}'_{inc}|$ as a function of $\nu'_{z,n}$ for the selected frequency values $\nu'_{x,n}$=0.5, 1.0 and 1.5. The aberrated curves have been labelled with the character a, the curves for a perfect system with the character p. Aberration coefficients: $\beta_0^0 = 1$, $\beta_3^1 = +i$, $\beta_3^{-1} = +i$.

integral over $\nu'_{z,n}$, associated with a full chord on the disk C_1 with $\psi = \pi$, is given by

$$\int I_b \, d\omega' \;=\; (-1)^l \, \frac{2\rho_0^2}{\nu'_{t,n}} \, \frac{\beta_0^0 \, \beta_k^{l\,*}}{k+1} \int\limits_0^{\left(1-\frac{\nu'_{t,n}}{2}\right)\nu'_{t,n}} \left[1 - \left(\nu'_{t,n}/2 + \nu'_{z,n}/\nu'_{t,n}\right)^2\right]^{1/2} U_k\left(\nu'_{t,n}/2 + \nu'_{z,n}/\nu'_{t,n}\right) d\nu'_{z,n} \; , \quad (35)$$

where we used that $f_3 \, \sin^2 \alpha'/\lambda = \rho_0^2/\nu'_{t,n}$. We remark that the integral above is the projection of the three-dimensional transfer function onto the plane $z = 0$. According to the Fourier slice theorem, this projection is equal to the (inverse) Fourier transform of the 3D transfer function with respect to the spatial frequency $\nu'_{z,n}$, evaluated at the point $z'_n = 0$. In optical terms, we obtain (part of) the two-dimensional x-y transfer function in an image plane with no defocus ($z'_n = 0$). Denoting the integral over I_b over the positive part of the $\nu'_{z,n}$-interval by $OTF_{b+}(\nu'_{x,n}, \nu'_{y,n}; z'_n)$ we obtain after the substitution $q = \nu'_{t,n}/2 + \nu'_{z,n}/\nu'_{t,n}$,

$$OTF_{b+}(\nu'_{x,n}, \nu'_{y,n}; 0) = 2\rho_0^2 \, (-1)^l \, \frac{\beta_0^0 \, \beta_k^{l\,*}}{k+1} \int\limits_{\nu'_t/2}^{1} \sqrt{1-q^2} \, U_k(q) \, dq \; . \quad (36)$$

With the substitution $q = \cos\phi$ we get the expression

$$OTF_{b+}(\nu'_{x,n}, \nu'_{y,n}; 0) = 2\rho_0^2 \, (-1)^l \, \frac{\beta_0^0 \, \beta_k^{l\,*}}{k+1} \int\limits_0^{\arccos(\nu'_t/2)} \sin\phi \, \sin[(k+1)\phi] \, d\phi \; . \quad (37)$$

and this yields the result

$$OTF_{b+}(\nu'_{x,n}, \nu'_{y,n}; 0) = \rho_0^2 \, (-1)^l \, \frac{\beta_0^0 \, \beta_k^{l\,*} \, \phi_0}{k+1} \, \{\mathrm{sinc}(k\phi_0) - \mathrm{sinc}[(k+2)\phi_0]\} \; , \quad (38)$$

with $\phi_0 = \arccos(\nu'_{t,n}/2)$.

The second contribution to $OTF_b(\nu'_{x,n}, \nu'_{y,n}; 0)$ comes from the $\nu'_{z,n}$-integration interval $[-\nu_{t,n}(1 - \nu'_{t,n}/2), 0]$ where the full chord is found on the disk C_0 with $\tau{=}\nu'_{t,n}/2 - \nu'_{z,n}/\nu'_{t,n}$ and $\psi = 0$ or π depending on the sign of τ. Proceeding along the same lines as above we have the result

$$OTF_{b-}(\nu'_{x,n}, \nu'_{y,n}; 0) = \rho_0^2 \, \frac{\beta_0^0 \, \beta_k^{l\,*} \, \phi_0}{k+1} \, \{\mathrm{sinc}(k\phi_0) - \mathrm{sinc}[(k+2)\phi_0]\} \; . \quad (39)$$

The contributions to the OTF-function coming from the integrations over I_c and I_d are calculated according to the same scheme. After summation of all analytic terms we obtain the final value of the transfer function.

5. Conclusion

It has been shown that the three-dimensional transfer function can be analytically evaluated in a relatively straightforward way, both for ideal and for aberrated imaging systems. From this 'master' function, by means of a partial inverse Fourier transformation with respect to one or two of its spatial frequency variables, we obtain useful transfer functions when imaging three-dimensional objects. As new analytic results we mention

a) the x-z transfer function evaluated as a function of the lateral off-set y' perpendicular to the imaged structure,

b) the classical x-y optical transfer function OTF in a plane perpendicular to the optical axis, both in focus and for an out-of-focus plane,

c) the axial z transfer function as a function of the lateral distance from a z-modulated line image.

In all these cases, analytic expressions were made available or semi-analytic solutions in terms of a series expansion with an infinite number of terms that can be truncated with the aid of a truncation rule that guarantees a desired accuracy of the result.

For aberrated imaging systems, the three-dimensional frequency transfer function is evaluated using a Zernike expansion of the complex lens pupil function. A result for the line-integral of a Zernike polynomial defined on the unit disk given by Cormack provides interesting expressions for the three-dimensional transfer function and for the classical two-dimensional OTF. In this paper we applied Cormack's result to weakly aberrated systems; to be able to use this result we used our radial scaling rule for Zernike polynomials. For severely aberrated imaging systems, a more involved scheme is needed that also uses the Zernike expansion coefficients of a shifted pupil function. This new procedure for transfer function evaluation using scaling, shifting and general multiplication operations on Zernike polynomials has been given in this paper; the details of these operations on Zernike polynomials can be collected from the recent literature. The analytic approach to optical transfer function calculation can replace, in many instances, the more common approach of numerical line or surface integration. The analysis provides the user with explicit physical relationships. In the case of analytic solutions a gain in calculation time is evident. For semi-analytic solutions with good convergence to the final value this is also a valid statement.

Appendices

Appendix A: Integral evaluation and series summation in the expression for the axial transfer function

In this Appendix we first evaluate the integral that appears after the equal sign in Eq.(17). The next step is the calculation of the number of terms that need to be included in the summation of Eq.(17) to obtain a certain accuracy.

A.1. Evaluation of the integral

In compact notation we write the integral after the summation sign of Eq.(17) as

$$I_m(w) = \int_{b_-}^{b_+} b^{2m-1} \sqrt{b^2 - \left(\frac{b^2}{2} + w\right)^2}\, db \;, \tag{A.1}$$

with $w = |\nu'_{z,n}| < 1/2$ and $b_\pm = 1 \pm \sqrt{1-2w}$. With the substitution $u = b^2$ we obtain after some rearrangement

$$I_m(w) = \frac{1}{4} \int_{u_-}^{u_+} (u - u_-)^{1/2}\, (u_+ - u)^{1/2}\, u^{m-1}\, du \;, \tag{A.2}$$

with the integration limits given by $u_\pm = 2[(1-w) \pm (1-2w)^{1/2}]$. We next substitute $t = (u-u_-)/(u_+ - u_-) \in [0,1]$, and we get

$$I_m(w) = 4(1-2w)\, u_-^{m-1} \int_0^1 t^{1/2}\, (1-t)^{1/2}\, (1 + a\, t)^{m-1}\, dt \;, \tag{A.3}$$

with a equal to $(u_+ - u_-)/u_-$. The remaining integral $I_{B,m}(w)$ with $m = 1, 2, \cdots$ can be cast into a series with Beta-integrals by using a power series expansion for the polynomial factor $(1+at)^{m-1}$ of the integrand,

$$I_{B,m}(w) = \sum_{k=0}^{m-1} \binom{m-1}{k} a^k \int_0^1 t^{k+1/2}\, (1-t)^{1/2}\, dt = \sum_{k=0}^{m-1} \binom{m-1}{k} \frac{\Gamma(k+3/2)\,\Gamma(3/2)}{\Gamma(k+3)}\, a^k \;. \tag{A.4}$$

This allows to write the final result for $I_m(w)$ with $m = 1, 2, \cdots$, as

$$I_m(w) = \pi\,(1-2w) \sum_{k=0}^{m-1} 2^k \binom{m-1}{k} \left(\frac{1}{2}.\frac{3}{3}.\, \cdots .\frac{2k+1}{k+2}\right)\, (1 - \sqrt{1-2w})^{2m-2-2k}\, (1-2w)^{k/2} \;. \tag{A.5}$$

The case $m = 0$ in Eq.(A.3) needs a special treatment. In terms of the hypergeometric function F, see [24], 15.2(i) and 15.6.1, we have

$$\begin{aligned} I_0(w) \;&=\; \frac{4(1-2w)}{u_-} \int_0^1 t^{1/2}\, (1-t)^{1/2}\, (1+at)^{-1}\, dt \\ &= \frac{\pi\,(1-2w)}{2\,u_-}\, F(1, 3/2\,; 3\,; -a) = \frac{\pi\,(1-2w)}{2\,u_-} \left(\frac{1}{2} + \frac{1}{2}\sqrt{1+a}\right)^{-2} \;, \end{aligned} \tag{A.6}$$

where [24], 15.4.17 has been used. From $a = (u_+ - u_-)/u_-$ and $u_\pm = b_\pm^2 = (1 \pm \sqrt{1-2w})^2$, we then readily get $I_0(w) = \pi\,(1-2w)/2$.

A.2. Truncation of the infinite series and accuracy of the partial sum

The semi-analytic expression in Eq.(17) for OTF_z is obtained by inserting the power series expansion $\sum_{m=0}^{\infty} (-z^2/4)^m/(m!)^2$ of the Bessel function $J_0(z)$. From the sharp form $m! \approx e^{-m}\, m^m\, \sqrt{2\pi m}$ of Stirling's formula, see [24], 5.11.1, it is seen that the terms in the series have modulus of the order $(e|z|/2m)^{2m}/2\pi m$. Thus, the maximum modulus of the terms, occurring for $m \approx |z|/2$, is of the order $\exp(|z|)/(\pi|z|)$, and there is rapid decay of the terms below 1 for $m \geq e|z|/2$. In the integral in Eq.(16), the worst case $|z| = 2\pi r'_n \nu'_{t,n}$ equals $4\pi r'_n$ (when $\nu'_{z,n} = 0$). For example, when computing with absolute accuracy 10^{-15}, one has that in worst case J_0 is approximated with absolute accuracy 10^{-5} when $r'_n \leq 2$ and when all terms in the power series with $m \leq 2\pi e r'_n + 5 = M$ are included.

Appendix B.0: Evaluation of the integral in Eq.(19)

Assume $0 < w \leq 1/2$. In the integral

$$I_m(s,w) = \int \frac{1}{s^2+v^2} \sqrt{s^2+v^2 - \left(\frac{s^2+v^2}{2} + w\right)^2}\, v^{2m}\, dv\,, \tag{B.1}$$

we carry out the substitution $u = s^2 + v^2$ to obtain

$$I_m(s,w) = \frac{1}{2} \int \frac{1}{u} \sqrt{u - \left(\frac{u}{2} + w\right)^2}\, \left(u - s^2\right)^{m-1/2}\, du\,, \tag{B.2}$$

with integration over all $u \geq s^2$ such that the square-root expression is non-negative. With $u_\pm = 2[1 - w \pm \sqrt{1-2w}]$, as in Appendix A, this is the case when $u_- \leq u \leq u_+$. Thus, we consider three cases,

$$\begin{array}{lll} a) & 0 < s \leq 1 - \sqrt{1-2w} \;\; : & u_- \leq u \leq u_+\,, \\ b) & 1 - \sqrt{1-2w} < s < 1 + \sqrt{1-2w} \;\; : & \overline{u} = s^2 < u < u_+\,, \\ c) & s \geq 1 + \sqrt{1-2w} \;\; : & \text{empty } u\text{-set} \end{array} \tag{B.3}$$

for the integration range in the integral in Eq.(B.2).

For the case in Eq.(B.3)a we substitute $q = [u - (u_+ + u_-)/2]\,/\,[(u_+ - u_-)/2] \in$ [-1,+1], and we get

$$I_m(s,w) = 2^{m-3/2}(1-2w) \int_{-1}^{+1} \frac{\left\{q\sqrt{1-2w} + 1 - w - s^2/2\right\}^{m-1/2}}{q\sqrt{1-2w} + 1 - w} \sqrt{1-q^2}\, dq\,. \tag{B.4}$$

We put

$$c = 1 - w - s^2/2\,, \qquad A = \frac{\sqrt{1-2w}}{1-w}\,, \qquad B = \frac{\sqrt{1-2w}}{1-w-s^2/2}\,, \tag{B.5}$$

and obtain

$$I_m(s,w) = 2^{m-3/2}\left(\frac{1-2w}{1-w}\right) c^{m-1/2} \int_{-1}^{+1} (1+Aq)^{-1}\,(1+Bq)^{m-1/2}\,\sqrt{1-q^2}\,dq\,. \tag{B.6}$$

From $0 < s \le 1 - \sqrt{1-2w}$ and $0 < w \le 1/2$, we have that $0 \le A < B \le 1$. To evaluate the remaining integral in Eq.(B.6), one approach is to develop $(1+Aq)^{-1}\,(1+Bq)^{m-1/2} = \sum_{j=0}^{\infty} d_j q^j$ into a power series converging for $|q| < 1$, and then to evaluate the integrals $\int_{-1}^{+1} q^j\,\sqrt{1-q^2}\,dq$ that show up in terms of Γ-functions. Alternatively, this integral can be expressed in terms of the Appell function F_1, see [24], 16.13-15, by the substitution $t = (1-q)/2 \in [0,1]$, so that

$$\begin{aligned} I_{m,a} &= \int_{-1}^{+1} (1+Aq)^{-1}\,(1+Bq)^{m-1/2}\,(1-q)^{1/2}\,(1+q)^{1/2}\,dq \\ &= 4(1+A)^{-1}(1+B)^{m-1/2} \int_0^1 t^{1/2}\,(1-t)^{1/2}\,\left(1-\frac{2At}{1+A}\right)^{-1}\,\left(1-\frac{2Bt}{1+B}\right)^{m-1/2} dt \\ &= \frac{\pi}{2}(1+A)^{-1}(1+B)^{m-1/2}\,F_1\left(3/2\,;1\,,-m+1/2\,;3\,;\frac{2A}{1+A},\,\frac{2B}{1+B}\right). \end{aligned} \tag{B.7}$$

Then using the series expansion [24], 16.13.1 of F_1, we get

$$I_{m,a} = \frac{\pi}{2}\,(1+A)^{-1}(1+B)^{m-1/2} \sum_{k,l=0}^{\infty} \frac{(3/2)_{k+l}}{(3)_{k+l}}\,\frac{(-m+1/2)_l}{l\,!}\left(\frac{2A}{1+A}\right)^k\,\left(\frac{2B}{1+B}\right)^l, \tag{B.8}$$

where we have used Pochhammer symbols, $(a)_0 = 1$ and $(a)_j = a(a+1)\cdots(a+j-1)$ for $j = 1, 2, \cdots$ and real a.

In the case of Eq.(B.3)b, we have that $|B| > 1$, and we must argue somewhat differently. We now have

$$\begin{aligned} I_m(s,w) &= \frac{1}{2}\int_{\overline{u}}^{u_+} \frac{1}{u}\,\sqrt{(u-\left(\frac{u}{2}+w\right)^2}\;\,(u-\overline{u})^{m-1/2}\;du \\ &= \frac{1}{4}\int_{\overline{u}}^{u_+} \frac{1}{u}\,\sqrt{u-u_-}\;\;(u-\overline{u})^{m-1/2}\;(u_+-u)^{1/2} du\,, \end{aligned} \tag{B.9}$$

where we have used that $u - (u/2+w)^2 = (u-u_-)(u_+-u)/4$. With

$$d = (u_+ - \overline{u})/2\,, \qquad u_0 = (\overline{u}+u_+)/2\,, \tag{B.10}$$

we substitute $q = (u - u_0)/d \in$ [-1,+1], and we get

$$I_m(s,w) = \frac{d^{m+1}}{4u_0}\,(u_0 - u_-)^{1/2} \int_{-1}^{1} (1+Cq)^{-1}\,(1+Dq)^{1/2}\,(1+q)^{m-1/2}(1-q)^{1/2}\,dq. \quad \text{(B.11)}$$

Here,

$$C = \frac{d}{u_0}\,, \qquad D = \frac{d}{u_0 - u_-}\,, \quad \text{(B.12)}$$

for which we have $0 < C < D < 1$ by the assumption $u_- < \overline{u} < u_+$ and the definition of d and u_0 in Eq.(B.10). We can now proceed as we did for the integral in Eq.(B.6) by developing $(1+Cq)^{-1}\,(1+Dq)^{1/2}$ as a power series $\sum_{j=0}^{\infty} e_j q^j$ converging for $|q| < 1$. The remaining integrals $\int_{-1}^{+1} q^j\,(1+q)^{m-1/2}\,(1-q)^{1/2}\,dq$ are now somewhat more awkward, but can still be evaluated in finite terms using Γ-functions. Alternatively, we can again express the remaining integral in Eq.(B.11) in terms of the Appell function F_1 and we get

$$\begin{aligned} I_{m,b} &= \int_{-1}^{+1} (1+Cq)^{-1}\,(1+Dq)^{1/2}\,(1+q)^{m-1/2}\,(1-q)^{1/2}\,dq \\ &= \frac{2^m\,(1/2)_m\,\pi}{(m+1)\,!}(1+C)^{-1}(1+D)^{1/2}\,F_1\left(3/2\,;1\,,-1/2\,;m+2\,;\frac{2C}{1+C},\,\frac{2D}{1+D}\right) \\ &= \frac{2^m\,(1/2)_m\,\pi}{(m+1)\,!}\,(1+C)^{-1}(1+D)^{1/2}\sum_{k,l=0}^{\infty}\frac{(3/2)_{k+l}}{(m+2)_{k+l}}\,\frac{(-1/2)_l}{l\,!}\left(\frac{2C}{1+C}\right)^k\left(\frac{2D}{1+D}\right)^l. \end{aligned} \quad \text{(B.13)}$$

The semi-analytic approach to evaluate the integrals in Eqs.(B.6),(B.11) by power series expansions of $(1+Aq)^{-1}(1+Bq)^{m-1/2}$ or $(1+Cq)^{-1}(1+Dq)^{1/2}$ yields a slightly faster converging series than the series in Eqs.(B.8),(B.13) that are based on the analytic result involving Appell functions. To produce Fig. 7, we used the power-series approach to evaluate the integrals in Eq.(19) and compared that with numerical integration of the integral in Eq.(18) using the trapezoidal rule. For small values of w, say $w \le 0.1$, the numbers A and B (or C and D) are very close to 1, so that the power series converge slowly, and then the numerical method is to be preferred over the power series method.

References

1. B. Roy Frieden, "Optical transfer of the three-dimensional object," J. Opt. Soc. Am. **57**, 56-66 (1967).
2. B. R. A. Nijboer, *The diffraction theory of aberrations*, Ph. D. dissertation (Rijksuniversiteit Groningen, 1942), J.B. Wolters, Groningen, downloadable from www.nijboerzernike.nl.

3. A. Maréchal, "Étude des effets combinés de la diffraction et des aberrations," Rev. Opt. 26, 257 (1947).
4. P.-M. Duffieux, *L'intégrale de Fourier et ses applications à l'optique*, privately published by Oberthur, Rennes, France (1946). English version: P.-M. Duffieux, *The Fourier transform and its applications to optics*, Wiley, New York, (1983).
5. A. Maréchal and P. Croce, "Un filtre de fréquences spatiales pour l'amélioration du contraste des images optiques," C. R. Acad. Sci. **237**, nr. 12, 607-609 (1953).
6. H. H. Hopkins, "On the diffraction theory of optical images," Proc. R. Soc. Lon. Ser.-A **217**, 408-432 (1953).
7. H. H. Hopkins, "The frequency response of a defocused optical system," Proc. R. Soc. Lon. Ser.-A **231**, 91-103 (1955).
8. H. H. Hopkins, "The application of frequency response techniques in optics," Proc. Phys. Soc. Lon. B **79**, 889-919 (1962).
9. M. Born and E. Wolf, *Principles of optics, electromagnetic theory of propagation, interference and diffraction of light*, Cambridge University Press, Cambridge (UK), 7th edition (1999).
10. G. Black and E. H. Linfoot, "Spherical aberration and the information content of optical images," Proc. R. Soc. Lon. Ser.-A **239**, 522 (1957).
11. A. M. Goodbody, "The influence of spherical aberration on the response function of an optical system," Proc. Phys. Soc. Lon. B **72**, 411 (1958).
12. A. M. Goodbody, "The influence of coma on the response function of an optical system," Proc. Phys. Soc. Lon. B **75**, 677-688 (1960).
13. M. De, "The influence of astigmatism on the response function of an optical system," Proc. R. Soc. Lon. Ser.-A **233**, 91-104 (1955).
14. N. Streibl, "Three-dimensional imaging by a microscope," J. Opt. Soc. Am. A **2**, 121-127 (1985).
15. C. J. R. Sheppard and X. Q. Mao, "Three-dimensional imaging in a microscope," J. Opt. Soc. Am. A **6**, 1260-1269 (1989).
16. M. Gu and C. J. R. Sheppard, "Three-dimensional imaging in confocal fluorescent microscopy with annular lenses," J, Mod. Opt. **38**, 2247-2263 (1991).
17. D. G. A. Jackson, M. Gu and C. J. R. Sheppard, "Three-dimensional optical transfer function for circular and annular lenses with spherical aberration and defocus," J. Opt.

Soc. Am. A **11**, 1758-1767 (1994).

18. M. Gu, *Advanced optical imaging theory*, Springer-Verlag, Berlin (2000).
19. C. J. R. Sheppard, M. Gu, Y. Kawata and S. Kawata, "Three-dimensional transfer functions for high-aperture systems," J. Opt. Soc. Am. A **11**, 593-598 (1994).
20. J. Philip, "Optical transfer function in three dimensions for a large numerical aperture," J. Mod. Opt. **46**, 1031-1042 (1999).
21. M. R. Arnison and C. J. R. Sheppard, "A 3D vectorial optical transfer function suitable for arbitrary pupil functions," Opt. Commun. **211**, 53-63 (2002).
22. A. Schoenle and S. W. Hell, "Calculation of vectorial three-dimensional transfer functions in large-angle focusing systems," J. Opt. Soc. Am. A **19**, 2121-2126 (2002).
23. P. A. Stokseth, "Properties of a defocused optical system," J. Opt. Soc. Am. **59**, 1314-1321 (1969).
24. F. W. J Olver, D. W. Lozier, R. F. Boisvert and C. W. Clark, *Handbook of Mathematical Functions* (Cambridge university Press, 2010).
25. C. J. R. Sheppard and M. Hole, "Three-dimensional optical transfer function for weak aberrations," J. Mod. Opt. **42**, 1921-1928 (1995).
26. A. M. Cormack, "Representation of a function by its line integrals, with some radiological applications," J. Appl. Phys. **34**, 2722-2727 (1963).
27. A. M. Cormack, "Representation of a function by its line integrals, with some radiological applications. II," J. Appl. Phys. **35**, 2908-2913 (1964).
28. S. R. Deans, *The Radon transform and some of its applications*, Wiley & Sons, New York (1983).
29. A. J. E. M. Janssen and P. Dirksen, "Computing Zernike polynomials of arbitrary degree using the discrete Fourier transform," J. Eur. Opt. Soc. Rapid **2**, 07012 (2007).
30. A. J. E. M. Janssen and P. Dirksen, "Concise formula for the Zernike coefficients of scaled pupils," J. Microlith. Microfab. Microsyst. **5**(3), 030501 (2006).
31. A. J. E. M. Janssen, "New analytic results for the Zernike circle polynomials from a basic result in the Nijboer-Zernike diffraction theory," J. Eur. Opt. Soc. Rapid **6**, 11028 (2011).
32. W. J. Tango, The circle polynomials of Zernike and their application in optics, Appl. Phys. **13**, 327332 (1977).
33. S. van Haver and A. J. E. M. Janssen, "Advanced analytic treatment and efficient

computation of the diffraction integrals in the extended Nijboer-Zernike theory," J. Eur. Opt. Soc. Rapid **8**, 13044 (2013).